RSC Advances

ROYAL SOCIETY OF CHEMISTRY

www.rsc.org/advances

Journal Name

ARTICLE

Enhancement of thermoelectric efficiency of doped PCDTBT polymer films

Jon Maiz[a], Miguel Muñoz-Rojo[a], Begoña Abad[a], Adam Wilson[b], Aurora Nogales[c], Diana-Andra Borca-Tasciuc[b], Theodorian Borca-Tasciuc[b], Marisol Martín-González*[a]*

Received 00th January 20xx,
Accepted 00th January 20xx

DOI: 10.1039/x0xx00000x

www.rsc.org/

Conjugated polymers may be used as thermoelectric materials due to their low thermal conductivity and have the advantageous characteristics of conventional polymers, such as low weight, non-toxicity and low cost. Here, a detailed investigation into the thermoelectric properties of PCDTBT films is reported. Moreover, in order to improve the thermoelectric properties of this polymer, $FeCl_3$ is used as a doping agent. For the most optimally doped film reported in this work, a power factor value of 24 μW m^{-1} K^{-2} is obtained at 150 °C. The different films were characterized by Wide-angle X-ray scattering (WAXS) experiments at different temperatures. In order to see the temperature effect, the thermoelectric power factor is measured as a function of temperature from (from RT to 150 °C). Thermal conductivity at room temperature is calculated with two independent methods which give values in agreement within the margin of uncertainty. The results obtained show promise and give insight to motivate future investigation into these types of carbazole derivates.

Introduction

In recent years, much effort has been invested in improving energy transport, especially in thermoelectric materials.[1] One of the most impactful applications of thermoelectricity is energy harvesting, wherein wasted heat is recovered to generate electricity, thus improving the overall efficiency of an energy cycle, or utilizing random ambient energy.[2, 3] The efficiency of thermoelectric devices is commonly reported as a dimensionless figure of merit, zT, which is expressed by: $zT = \sigma \cdot S^2 \cdot T/\kappa$ [Eq.1], where T is the absolute temperature, σ is electrical conductivity, S is the Seebeck coefficient, and κ is thermal conductivity. The Seebeck coefficient is a measurement of the amount of potential induced per difference in temperature and mathematically, it is defined as $\Delta S = \Delta V/\Delta T$ [Eq.2].

The terms $\sigma \cdot S^2$ are commonly grouped together and are known as the power factor. Since inorganic materials such as several alloys and intermetallics based on Bi, Te, Sb, Pb, *etc.*, normally

[a] IMM-Instituto de Microelectrónica de Madrid (CNM-CSIC), Isaac Newton 8, PTM, E-28760 Tres Cantos, Madrid, Spain. Email: j.maiz@csic.es (J.M.); marisol@imm.cnm.csic.es (M.M-G.).
[b] Department of Mechanical, Aerospace and Nuclear Engineering, Rensselaer Polytechnic Institute, 110 8th Street, Troy, NY 12180 USA
[c] Instituto de Estructura de la Materia (IEM-CSIC), Serrano 121, 28006 Madrid, Spain.

have high *σ,* extensive research has been done on such materials.[2] Attempting to suppress thermal conductivity without sacrificing the electrical conductivity has been one of the main strategies to enhance *z*T values of inorganic thermoelectric materials.[4-7] On another hand, organic materials, such as semiconductor polymers, exhibit low *κ,* which could compensate for the decrease in zT caused by their low *σ*. Moreover, organic materials are abundant, light-weight, flexible, solution-processable and in most cases low-cost. Nowadays, the highest zT values obtained are starting to get higher than 1.5 in some families of inorganic materials. However, the real fact is that, while zT in inorganic materials has increased by a factor of 3 or 4 in the last years, mostly via nanostructuration. In the case of organic materials the increase in zT has been of several orders of magnitude. A few years ago the figure of merit of most conducting polymers were of the order of 10^{-4}, nowadays the best values are reaching 0.5.

Recently, it has been demonstrated that the p-type material poly(3,4-ethylenedioxythiophene) (PEDOT) exhibits a high *z*T value of 0.42 at room temperature,[3] which is the highest reported value of zT among organic materials to date. On the other hand, in inorganic materials the thermoelectric materials most used at temperatures close to the room one (< 450 K), are Bi_2Te_3 y Sb_2Te_3, with zT >1.

Some of the most commonly studied polymers have been: polyaniline (PANI),[8-10] polyalkyl thiophenes,[11, 12] poly(3,4-ethylenedioxythiophene) (PEDOT),[3, 13-18] polypyrrole (PPy)[10, 19] and poly(2,7-carbazolyenevinylene).[20, 21] One way to improve electrical conductivity in conjugated polymers is to introduce extra charge carriers, such as polarons and bipolarons, by electrochemical or chemical doping. These carriers favor charge transfer along the polymer chains by hopping. However, doping may have an adverse effect on the Seebeck coefficient by driving the Fermi level closer to the conduction band.[13, 20, 22, 23] For this reason, optimization of both parameters should be performed to obtain the maximum thermoelectric efficiency.

Here, we investigate the thermoelectric properties of iron-doped poly [N-9'-heptadecanyl-2,7carbazole-alt-5,5-(4',7'-di-2-thienyl-2',1',3-benzothiadizole)] (PCDTBT) films. The dopant is introduced as iron trichloride ($FeCl_3$), which is optimal for doping due to its oxidizing properties.[20] During the oxidation process the resulting positive charges on the polymer chains are balanced by the presence of $FeCl_4^-$ counter-ions.[21, 24] Each of *σ*, *κ,* and *S* are measured to find the zT of the PCDTBT films under different doping conditions.

Experimental

Fabrication of non-doped PCDTBT films.

The non-doped films of PCDTBT were prepared *via* drop casting on glass substrates. The glass substrates were cleaned in an ultrasonic acetone bath for 5 min. Then, poly [N-9'-heptadecanyl-2,7carbazole-alt-5,5-(4',7'-di-2-thienyl-2',1',3-benzothiadizole)] (PCDTBT) supplied by Solaris Chem Inc., with weight-average molecular weight (M_w) of 53000 g mol^{-1} and a polydispersity index of 1.5, was dissolved in chloroform at room temperature to produce a 50 mg mL^{-1} solution. Afterwards, the polymer solution was drop-casted on a glass substrate and the chloroform solvent was allowed to evaporate at room temperature for 24 h. A film of PCDTBT was formed with a thickness around 3 µm and roughness of around 90 nm (measured by Veeco Dektak profilometer).

Fabrication of doped PCDTBT films.

The PCDTBT films were doped using the doping agent $FeCl_3$. Similarly to the non-doped film, pure PCDTBT/chloroform solutions were prepared and afterwards we dropped wise it into different concentrations of $FeCl_3$/chloroform solutions. Using the same drop-casting procedure as for the non-doped case, polymer films with 0.5, 1, 1.5 and 2 monomer units per $FeCl_4^-$ doping levels on glass substrates were obtained. The thicknesses of these films were ranging between 3 µm and 5 µm and roughness of around 400 nm were found (measured by Veeco Dektak profilometer).

Structural characterization

Bulk PCDTBT was evaluated via Thermogravimetric analysis (TGA) performed on a Q500 TA Instruments TGA system, using air stream as the purge gas, at a heating rate of 10 °C/min in the range of 0-900 °C. Calorimetric measurement of bulk PCDTBT sample was conducted in a Perkin-Elmer 8500 differential scanning calorimeter to measure temperature transitions in the heating and cooling mode from the room temperature at 20 °C min^{-1}. The structural characterization was carried out in Wide-angle X-ray scattering (WAXS) experiments in a geometry in which the wave vector, *Q*, was parallel to the long axis of sample in reflection geometry using a Philips X'Pert diffractometer. Moreover, WAXS experiments were also carried out in transmission geometry with the X-ray beam traveling along the direction perpendicular to the sample surface using a Bruker AXS Nanostar X-ray scattering instruments, so that *Q* was nearly perpendicular to the long axis of the sample. In the scheme 1 a schematic representation of the set-ups can be observed in order to interpret the experiments performed.

Physical properties characterization

The hole mobility of the best doped sample was measured by Hall effect measurement system (commercial ECOPIA set-up) in order to compare with that result gave by Sigma Aldrich for the raw PCDTBT.

a) Power factor measurements.

The electrical conductivity of the doped films was measured by the four probe Van der Pauw (VdP) method.[25] The four probes are positioned at each corner of the sample while measuring the voltage and current respectively between sets of them.[25]

To measure the Seebeck coefficient, a controlled temperature gradient was applied along the sample while measuring the resulting voltage drop.[26]

Moreover, for doped PCDTBT films, the electrical conductivity and the Seebeck coefficient were cross-checked with LSR-3 LINSEIS commercial equipment. These measurements were

performed from room temperature (RT) to 150 °C. The PCDTBT non-doped film was not able to be measured by this method, as the high electrical resistance was over the measurement limit of the system.

b) Thermal properties.

Thermal conductivity measurements were performed by two independent methods: the photoacustic technique[27] and the 3ω-SThM (Scanning Thermal Microscopy)[28] method based on Scanning Probe Joule heating based thermal microscopy.

The 3ω-SThM has been used to determine the thermal conductivity of organic and inorganic nanostructures, such as films[29] or nanowires.[28, 30] This technique uses a thermo-resistive probe that is heated by Joule effect when passing an electrical current through it.

When approaching the sample surface, a heat flux is exchanged between the probe and the surface of the sample. As a consequence, the temperature of the probe changes and so does its electrical resistance.

The third harmonic, 3ω, of the electrical response of the probe can be then expressed as a function of the thermal conductivity of the sample under study.[31, 32] In this work, the setup is identical to the one showed in reference [32]. A Wollaston probe[33] and an Atomic Force Microsocope (AFM) from Nanotec® were used to carefully position the probe on the surface of the films. An external UHF lock-in amplifier from Zurich instruments was used to record the 3ω voltage.

The thermal conductivity at room temperature in the cross-plane direction was also measured by a system based on the photoacoustic technique, as a crosscheck. An incident modulated radiation from a fiber-couple laser diode of 980 nm with an optical power of 260 mW periodically heats the sample.

Acoustic waves are created as the air in contact with the surface expands and contracts, similar to a thermal piston. A microphone is used to detect the acoustic waves in such a way that the thermal properties of the sample can be obtained by comparing the incident modulated signal from the laser with the recorded signal and fitting the signal to a multilayer model developed by Hu et al.[34] The sample was metallized by an 80 nm titanium layer via electron-beam evaporation in order to absorb the laser beam.

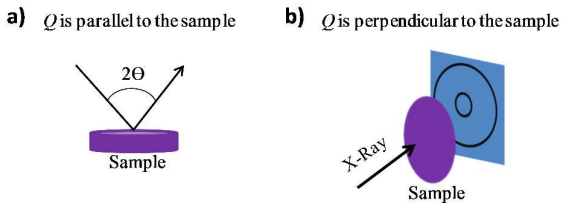

Scheme 1. Schematic representations of WAXS experiments (a) in reflection geometry and (b) experiment in transmission geometry.

Results and discussion

Structural characterization.

Before the film preparation step, the bulk polymer thermal stability is evaluated by TGA. The PCDTBT shows a good thermal stability.[35] In the first heating run, a weight loss is observed at 315 °C, which is attributed to the decomposition of the lateral alkyl chains that are positioned in the carbazole group [Figure 1 (a)]. At higher temperature the thermogram shows two different peaks, at 383 °C and 506 °C. The first peak corresponds to the carbazole group and the second one to the thiophene and benzothiadiazole groups. DSC experiments were carried out in order to observe the thermal behavior of the PCDTBT samples [Figure 1 (b)].

The observed temperatures (T_m = 120 °C and T_m = 277 °C) are used as a reference when the electrical conductivities are studied, as shown below. Both of these melting temperatures are like order-disorder transitions for each monomer; no crystallization peaks were observed during the cooling process (not shown here, heating and cooling sweeps were performed).

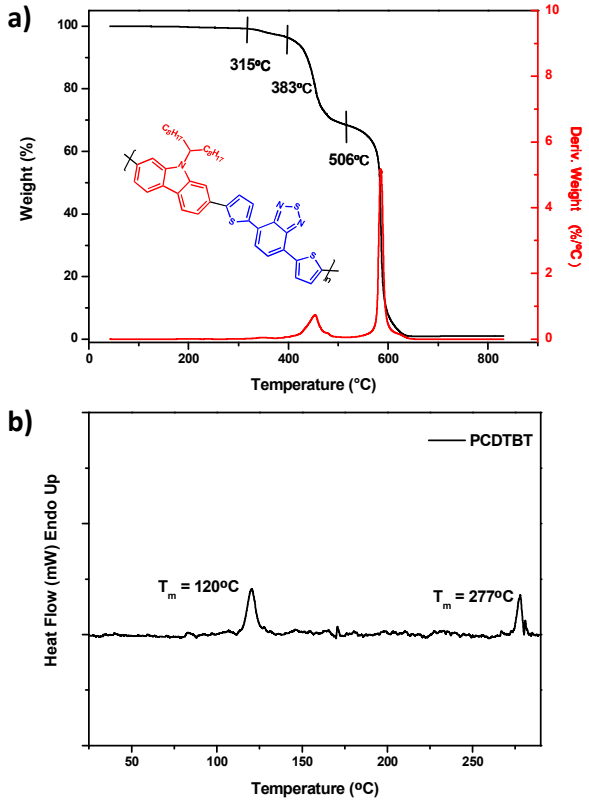

Figure 1. (a) Thermogravimetric analysis (TGA) of PCDTBT bulk sample and (b) heat flow vs temperature during non-isothermal sweep of bulk PCDTBT sample and at 20 °C min^{-1}.

Several studies have demonstrated that structural parameters can influence the charge transport properties in conjugated polymers.[36-39] For instance, orientation and structural organization of the polymers may play a crucial role.[40-42] In order to see what kind of process takes place in the PCDTBT complex structure, WAXS experiments were carried out (Figure 2). Moreover, in order to clarify the order-disorder peaks observed by DSC, the WAXS patterns were collected at temperatures just before and after the endothermic processes observed, up to 280 °C.

X-ray data suggest a lamellar packing for the undoped and the 1:1 doped PCDTBT films. The peak around q = 0.31 A^{-1} corresponds to a layering distance of *d* = 19.6 Å between sheets of each one of polymer chains that are packed in the plane, perpendicular to their longitudinal axes.

The second broader peak, near q = 1.53 A^{-1}, corresponds to a *d*-spacing of 4 Å, and could be attributed to the distance between the polymer chains within the layered planes.[21, 43] This distance has been attributed to the π-π stacking in PCDTBT[43] induced by the benzothiadiazole unit. The first (sharpest) peak can be observed both in the undoped and in the doped film, as well in both parallel and perpendicular configurations [Figure 2(a) and (b)]. There is a slight difference between undoped and doped samples, where the peaks in the doped films are slightly displaced to higher angles, namely to lower d-spacing, indicating that doping produces a more compact packing of the layers.

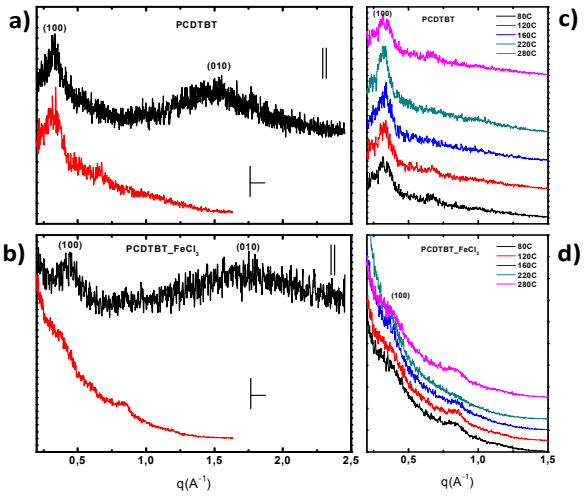

Figure 2. WAXS diffractograms of (a) PCDTBT thin film and (b) doped PCDTBT thin film in which the wave vector, q, was parallel (‖) and perpendicular (⊢) to sample surface. WAXS patterns at different temperatures of (c) PCDTBT thin film in which the wave vector, q, was perpendicular to the surface, five diffractograms in the temperature range 80-280 °C were taken and (d) doped PCDTBT thin film in which the wave vector, q, was perpendicular to the surface, five diffractograms in the temperature range 80-280 °C were taken.

Apparently, an isotropic behavior is observed in all the samples prepared. The fact that on the transmission experiments, the broad [010] peak associated to the π-π stacking is not observed is a clear indication of the configuration of the polymer chains parallel to the surface, even in these macroscopic films, similar to what is observed in thin films by grazing incidence.[43] Figure 2 (c) and (d) show the evolution with temperature of the diffraction pattern in transmission geometry for the undoped and doped samples, respectively. In the undoped sample, besides the main peak at q = 0.31 A^{-1}, a weak peak is observed around q = 0.62 A^{-1}, that can be attributed to a second order of the main peak, indicating a well-defined layer structure. The second order disappears at T > 140 °C, and the main peak becomes sharper. When comparing with the DSC trace [Figure 1 (b)], the disappearance of the second order corresponds to temperatures above the endothermic peak at T = 120 °C in the DSC, and that some authors have attributed to the glass transition of PCDTBT.[44] After the second endothermic peak (T = 277 °C), due to a recombination of the polymer chains, the second order appears again indicating a well-defined layer structure. In the doped samples, although features are somehow hidden by the strong scattering coming from residual Fe ions, the main peak is shifted at higher q values (around q = 0.39 A^{-1}) angles when compared with the undoped sample. This observation indicates that $FeCl_3$ induces a more compact layer structure of PCDTBT, and this can be corroborated from the position of the second order peak, located around q = 0.80 A^{-1}. WAXS experiments allow to conclude that the layer spacing shifts from d = 20 Å in the undoped sample to d = 16 Å in the doped samples.

As we expect, there is not a simple melting process observed, however an order-disorder process of the crystals can be intuited due to the increase and the decrease of the peak intensities.

Thermoelectric properties.

Figure 3 (a) and (b) show the results obtained for the Seebeck coefficient, electrical conductivity and the power factor at room temperature for the PCDTBT films with and without doping. As can be seen in Figure 3 (a) the highest electrical conductivity is obtained from the doped PCDTBT film with one monomer unit per $FeCl_3$ molecule. Positive values of the Seebeck coefficient are obtained for all doped films, indicating a p-type conduction (hole conduction). Moreover, the electrical conductivity increases up to nine orders of magnitude with the addition of the doping agent from 1.10^{-7} S cm^{-1} for the undoped PCDTBT film to 63 S cm^{-1} for the 1:1 doped PCDTBT film. Figure 3 (b) shows the doping dependence of the power factor. The best balance between the electrical conductivity and Seebeck coefficient led to a power factor of 9 μW m^{-1} K^{-2} for one monomer unit per $FeCl_3$ doping level.

The electrical conductivity dependence with the doping level can be explained in terms of trapping. According to Bubnova *et al*[45], when the doping level is low the extra introduced carriers into the polymer chains remain localized into the traps created

by the counter-ions, and the mobility is not sharply increased. When the doping is increased, and hence, the counter-ions are also increased, the Coulomb traps start to overlap and the energy barriers between them decrease. Then, an energy disorder decrease would take place so that both mobility and Seebeck coefficient would increase.

However, if the doping level is further increased, the electrostatic forces between counter-ions increase, and so does their distance and therefore the charge hopping is not facilitated. The Seebeck coefficient decreases as the doping level is decreased probably due to an increase in the carrier density as Snyder *et al.* explained.[46]

Moreover, the electrical conductivity and Seebeck coefficient were measured between 40 °C to 140 °C only for the PCDTBT doped films. That can be explained in terms of the low charge carrier density, which is characteristic of conjugated polymers (< 10^{14} $|e|$ cm^{-3})[45] since electrical conductivity is given by the expression $\sigma = n|e|\mu$ [Eq.3] where n is the charge carrier density, $|e|$ is the elementary charge and μ is the mobility of the charge carriers.

As shown in Figure 4 (a) and (b), the conductivity and Seebeck coefficient are thermally activated in all doped samples, which the system must overcome an energy barrier in order for the process to go forward. Moreover, the electrical conductivity increases when the temperature is increased which is the typical semiconductor behavior, reaching a value as high as 110 S cm^{-1} for the 1:1 doped sample at 150 °C. As a consequence, the power factor increases when the temperature also increases, as it is observed in figure 4 (c). For the best doped film (one monomer unit per $FeCl_4^-$) values up to 24 μW m^{-1} K^{-2} are obtained at 150 °C. This sample presents a Seebeck coefficient of 47 μV K^{-1}, but it is worthy to note that a great enhancement of the Seebeck coefficient is reached for doping levels ≥ 1.5:1 of given a value of 60-70 μV K^{-1} which is compensated in the final power factor by a reduction in the electrical conductivity in comparison with the 1:1 sample. This polymer can be used up to 120 °C, where the first order-disorder transition is observed indicating a not well defined layer structure as we observed in the WAXS diffractograms.

The electrical conductivity is observed to behave as $\sigma = \sigma_0 e^{-Ea/kT}$ [Eq.4]. With increasing disorder the activation energy E_a rises while the pre-exponential factor σ_0 decreases.[12] As plotted in Figure 5 the activation energy is related to the doping level: 40 meV, 9 meV, 72 meV, and 84 meV for 0.5, 1, 1.5 and 2 monomer units per $FeCl_3$ molecule, respectively. The activation energy is reduced when decreasing the doping level from 2:1 to 1:1, i.e., when the samples are more doped, since the carrier density is increased. Finally, the activation energy increases again when the lowest doping level is reached, 0.5:1, since the electrostatic forces between counter-ions increase which make the electronic transport more difficult. As shown before, all doped samples are thermally activated and as a consequence the electrical conductivity increases when the activation energy decreases.

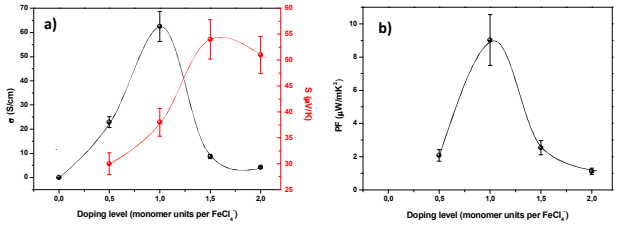

Figure 3. (a) Electrical conductivity (black line) and Seebeck coefficient (red line) for undoped and doped PCDTBT films as a function of the doping level. (b) Power factor for the doped PCDTBT films as a function of the doping level at room temperature.

The temperature dependence of the Seebeck coefficient could be used as an indicator of the charge transport mechanism in semiconductor materials. The Seebeck coefficient of organic semiconductors can present different temperature dependences[45]. As seen in Figure 4 (b) the Seebeck coefficient is thermally activated, showing an increase in its magnitude as increasing the temperature for all the doped samples. In the case of the conventional semiconductors, i.e., inorganic semiconductors, the transport mechanism is described in terms of energy bands and the 1/T dependence of the Seebeck coefficient is the typical behavior.

In the case of the organic semiconductor where no band structure is present and this temperature dependence occurs, another kind of transport phenomena is taking place. It is called nearest-neighbor hopping thermopower which follows the expression:[47]

$$S = -[(E_A')/qT] + A \qquad \text{Eq. 5}$$

An analysis of the Seebeck coefficient as a function of the 1/T allows one to obtain a linear trend whose slope corresponds to the activation energy, E_A', and the intercept, A, corresponds to a temperature independent kinetic term.

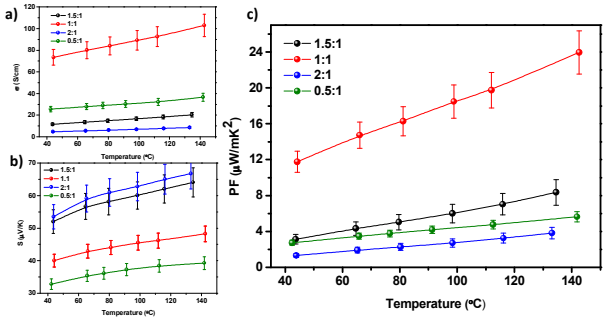

Figure 4. Temperature dependence of (a) electrical conductivity, (b) Seebeck coefficient and (c) power factor for the different doping levels in the PCDTBT films.

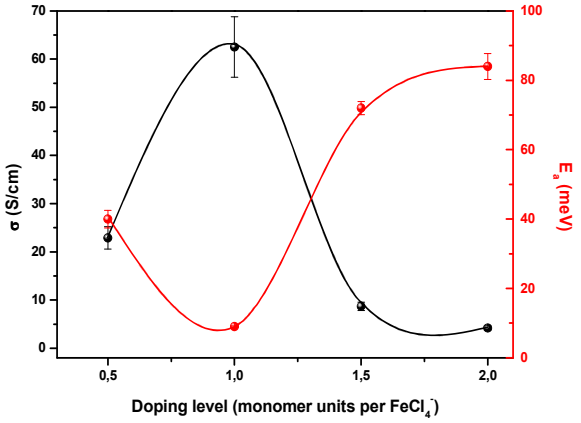

Figure 5. Evolution of the electrical conductivity and the activation energy E_a versus doping level.

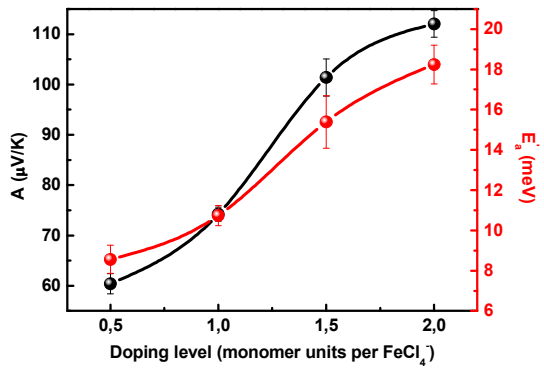

Figure 6. The evolution of the Seebeck coefficient (E_A') and its $1/T$ = 0 intercept (A) with doping concentration.

As seen in Figure 6, the activation energy increases as the doping level is increased. On the other hand, the temperature independent term undergoes a sharp change when doping is varied as seen in doped P3HT. Both magnitudes show the same dependence with the doping level as the trend found by Xuan *et al* for P3HT doped with $NOPF_6$.[12]

The raw PCDTBT exhibits a hole mobility of $6x10^{-5}$ cm^2 V^{-1} s^{-1}. Depending on the doping level, the hole mobility can vary between 5-10 orders of magnitude. In this work, we have measured the hole mobility by the Hall effect measurement system to be $1.5x10^2$ cm^2 V^{-1} s^{-1} for the best doped sample (1 monomer unit per $FeCl_4^-$).

Figure 7 shows the dependence of the thermal conductivity with the doping level. Two different techniques were used to measure the undoped PCDTBT film (PA and 3ω-SThM) observing good agreement between them, within the error bar. After this double-checks in the undoped PCDTBT samples, the doped samples were measured by the 3ω-SThM system.

The value for the undoped film is 0.25±0.04 W m^{-1} K^{-1}, which agrees well with a cross-check measurement taken by PA (0.20±0.03 W m^{-1} K^{-1}). In the undoped polymer, its thermal conductivity is mainly dominated by phonons, $k \approx k_{lattice}$, and it is expected to be that low because of the typical characteristics of the polymers. However, when doping the PCDTBT with $FeCl_3$, not only the lattice, but also the electronic terms contribute to the total thermal conductivity, $k = k_{electronic} + k_{lattice}$. Similarly to what happened with the electrical conductivity (Figure 5) the 1:1 doping shows the maximum thermal conductivity, 1 W m^{-1} K^{-1}.

This can be related to the lower energy barriers observed in this case, which increase the mobility of electrons and so increase the electronic thermal conductivity. However, although the trend in the total thermal conductivity for other doped levels becomes slightly smaller than for the 1:1 doped level, it is not that drastically reduced as the electrical conductivity case. In reference [48], the transport properties of PEDOT polymers were determined for different polymerization processes.[48] The influence of the electronic contribution to the total thermal conductivity was studied and compared with the Wiedemann-Franz law.[48] In these measurements, variations of σ from tens to several hundred S cm^{-1} showed a general dependence of k with σ. Despite this trend, one must note that the variation in k is smaller than the variation in σ. Taking this into account, in our measurements much smaller

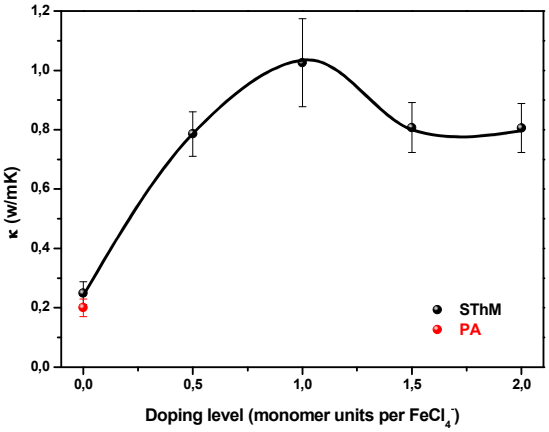

Figure 7. Evolution of thermal conductivity versus doping level measured by 3ω-SThM technique (black dots and line). Measured thermal conductivity for undoped PCDTBT film by photoacustic system (red dot).

variations of σ with the doping were obtained, which make the thermal conductivity trend less clear, but similar within the error, because of possibly similar influence of the electronic thermal conductivity term in the different doped samples.

Our results show that for the $FeCl_3$ levels of doping used in PCDTBT samples, we can vary the electrical conductivity without modifying much the total thermal conductivity of the samples. From the point of view of thermoelectricity, these are good news as we can keep a relatively low value of the thermal conductivity while improving the power factor of the polymer. Other doping elements, thermal treatments or different ways of growing the polymer films could be used in order to try to achieve higher values of the power factor with relatively low thermal conductivities.

Figure 8 shows the figure of merit for each sample prepared.

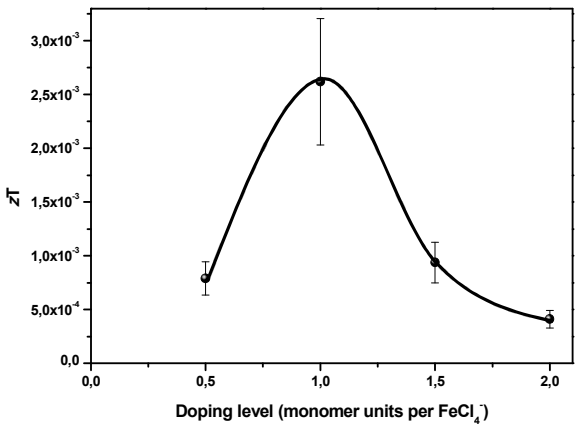

Figure 8. Thermoelectric Figure of Merit versus doping level.

It is interesting to see that the best doping sample reaches up to $(2.6\pm0.6).10^{-3}$ in zT value at room temperature. The best reported values[12] for these types of carbazoles were around 8.10^{-5}, so there is an enhancement of two orders of magnitude in the Figure of Merit for this carbazole derivate.

Conclusions

In summary, PCDTBT polymer films prepared by drop-casting (both undoped and doped with $FeCl_3$) were studied. The doped film, which exhibited the highest thermoelectric efficiency had one monomer per one doping molecule. For this sample, a relatively high value of electrical conductivity for this type of material was observed. Additionally, the value of Seebeck coefficient was found to be close to that for materials of similar composition as Leclerc *et al.* reported. Moreover, the electrical conductivity increases when the temperature is increased which is the typical semiconductor behavior, reaching a value as high as 110 S cm^{-1} for the 1:1 doped sample at 150 °C. The thermal conductivity also was measured in this work by two different techniques observing good agreement between them for the undoped films. For the doped films, thermal conductivity was observed to increase up to a plateau value of 1 W m^{-1} K^{-1}. Our results show that for the $FeCl_3$ levels of doping used in PCDTBT samples, we can vary the electrical conductivity without greatly modifying the value of thermal conductivity of the samples.

Acknowledgements

This work has been supported by ERC Starting Grant Nano-TEC number 240497, Nanotherm Consolider CSD-2010-00044 project and PHOMENTA project MAT2011-27911. We gratefully acknowledge funding from the US Department of Energy, Office of Basic Energy Sciences through the S3TEC Energy Frontiers Research Center (T.B.T.), and NSF IRES grant #1028071 and the Fulbright for financial support towards this work (A.W., D.A.B.T and D.B.T.).

Notes and references

1 1. X. Chen, C. Li, M. Gratzel, R. Kostecki and S. S. Mao, *Chemical Society Reviews*, 2012, **41**, 7909-7937.

2 2. M. Martín-González, O. Caballero-Calero and P. Díaz-Chao, *Renewable and Sustainable Energy Reviews*, 2013, **24**, 288-305.

3 3. G. H. Kim, L. Shao, K. Zhang and K. P. Pipe, *Nat Mater*, 2013, **12**, 719-723.

4 4. M. S. Dresselhaus, G. Chen, M. Y. Tang, R. G. Yang, H. Lee, D. Z. Wang, Z. F. Ren, J. P. Fleurial and P. Gogna, *Advanced Materials*, 2007, **19**, 1043-1053.

5 5. C. Wan, Y. Wang, N. Wang, W. Norimatsu, M. Kusunoki and K. Koumoto, *Science and Technology of Advanced Materials*, 2010, **11**, 044306.

6 6. D. J. Voneshen, K. Refson, E. Borissenko, M. Krisch, A. Bosak, A. Piovano, E. Cemal, M. Enderle, M. J. Gutmann, M. Hoesch, M. Roger, L. Gannon, A. T. Boothroyd, S. Uthayakumar, D. G. Porter and J. P. Goff, *Nat Mater*, 2013, **12**, 1028-1032.

7 7. J. Tang, H.-T. Wang, D. H. Lee, M. Fardy, Z. Huo, T. P. Russell and P. Yang, *Nano Letters*, 2010, **10**, 4279-4283.

8 8. B. Abad, I. Alda, P. Diaz-Chao, H. Kawakami, A. Almarza, D. Amantia, D. Gutierrez, L. Aubouy and M. Martin-Gonzalez, *Journal of Materials Chemistry A*, 2013, **1**, 10450-10457.

9 9. Q. Yao, Q. Wang, L. Wang and L. Chen, *Energy & Environmental Science*, 2014, **7**, 3801-3807.

10 10. N. Mateeva, H. Niculescu, J. Schlenoff and L. R. Testardi, *Journal of Applied Physics*, 1998, **83**, 3111-3117.

11 11. W. Shi, J. Chen, J. Xi, D. Wang and Z. Shuai, *Chemistry of Materials*, 2014, **26**, 2669-2677.

12 12. Y. Xuan, X. Liu, S. Desbief, P. Leclère, M. Fahlman, R. Lazzaroni, M. Berggren, J. Cornil, D. Emin and X. Crispin, *Physical Review B - Condensed Matter and Materials Physics*, 2010, **82**.

13 13. O. Bubnova, Z. U. Khan, H. Wang, S. Braun, D. R. Evans, M. Fabretto, P. Hojati-Talemi, D. Dagnelund, J. B. Arlin, Y. H. Geerts, S. Desbief, D. W. Breiby, J. W. Andreasen, R. Lazzaroni, W. M. Chen, I. Zozoulenko, M. Fahlman, P. J. Murphy, M. Berggren and X. Crispin, *Nature Materials*, 2014, **13**, 190-194.

14 14. O. Bubnova, Z. U. Khan, A. Malti, S. Braun, M. Fahlman, M. Berggren and X. Crispin, *Nat Mater*, 2011, **10**, 429-433.

15 15. T. Park, C. Park, B. Kim, H. Shin and E. Kim, *Energy & Environmental Science*, 2013, **6**, 788-792.

16 16. M. Culebras, C. M. Gomez and A. Cantarero, *Journal of Materials Chemistry A*, 2014, **2**, 10109-10115.

17 17. N. Massonnet, A. Carella, O. Jaudouin, P. Rannou, G. Laval, C. Celle and J.-P. Simonato, *Journal of Materials Chemistry C*, 2014, **2**, 1278-1283.

18 18. N. Massonnet, A. Carella, A. de Geyer, J. Faure-Vincent and J.-P. Simonato, *Chemical Science*, 2015, **6**, 412-417.

19 19. L. Wang, F. Liu, C. Jin, T. Zhang and Q. Yin, *RSC Advances*, 2014, **4**, 46187-46193.

20 20. M. Culebras, C. Gómez and A. Cantarero, *Materials*, 2014, **7**, 6701-6732.

21 21. R. B. Aïch, N. Blouin, A. Bouchard and M. Leclerc, *Chemistry of Materials*, 2009, **21**, 751-757.

22 22. B. T. McGrail, A. Sehirlioglu and E. Pentzer, *Angewandte Chemie International Edition*, 2014, DOI: 10.1002/anie.201408431, n/a-n/a.

23 23. Q. Zhang, Y. Sun, W. Xu and D. Zhu, *Advanced Materials*, 2014, **26**, 6829-6851.

24 24. I. Lévesque, X. Gao, D. D. Klug, J. S. Tse, C. I. Ratcliffe and M. Leclerc, *Reactive and Functional Polymers*, 2005, **65**, 23-36.

25 25. L. J. van der Pauw, *Philips Res. Repts*, 1958, **13**, 1-9.

26 26. H.-J. Kim, J. R. Skuza, Y. Park, G. C. King, S. H. Choi and A. Nagavalli, *NASA Technical Reports Server (NTRS)*, 2012, **NASA/TM-2012-217791**.

27 27. K. G. Biswas, T. D. Sands, B. A. Cola and X. Xu, *Applied Physics Letters*, 2009, **94**, -.

28 28. M. Muñoz Rojo, S. Grauby, J. M. Rampnoux, O. Caballero-Calero, M. Martin-Gonzalez and S. Dilhaire, *Journal of Applied Physics*, 2013, **113**.

29 29. S. Rausch, D. Rauh, C. Deibel, S. Vidi and H. P. Ebert, *Int J Thermophys*, 2013, **34**, 820-830.

30 30. M. M. Rojo, J. Martin, S. Grauby, T. Borca-Tasciuc, S. Dilhaire and M. Martin-Gonzalez, *Nanoscale*, 2014, **6**, 7858-7865.

31 31. M. M. Rojo, O. C. Calero, A. F. Lopeandia, J. Rodriguez-Viejo and M. Martín-Gonzalez, *Nanoscale*, 2013, **5**, 11526-11544.

32 32. T. Borca-Tasciuc, D. A. Borca-Tasciuc and G. Chen, Annual IEEE Semiconductor Thermal Measurement and Management Symposium, San Jose, CA, 2005.

33 33. A. Stranz, A. Waag and E. Peiner, *J Mater Res*, 2011, **26**, 1958-1962.

34 34. H. Hu, X. Wang and X. Xu, *Journal of Applied Physics*, 1999, **86**, 3953-3958.

35 35. S. Cho, J. H. Seo, S. H. Park, S. Beaupré, M. Leclerc and A. J. Heeger, *Advanced Materials*, 2010, **22**, 1253-1257.

36 36. H. W. Wang, E. Pentzer, T. Emrick and T. P. Russell, *ACS Macro Lett.*, 2014, **3**, 30-34.

37 37. F. Provencher, N. Bérubé, A. W. Parker, G. M. Greetham, M. Towrie, C. Hellmann, M. Côté, N. Stingelin, C. Silva and S. C. Hayes, *Nat. Commun.*, 2014, **5**.

38 38. M. Scarongella, A. A. Paraecattil, E. Buchaca-Domingo, J. D. Douglas, S. Beaupré, T. McCarthy-Ward, M. Heeney, J. E. Moser, M. Leclerc, J. M. J. Fréchet, N. Stingelin and N. Banerji, *J. Mater. Chem. A*, 2014, **2**, 6218-6230.

39 39. A. A. Y. Guilbert, M. Schmidt, A. Bruno, J. Yao, S. King, S. M. Tuladhar, T. Kirchartz, M. I. Alonso, A. R. Goñi, N. Stingelin, S. A. Haque, M. Campoy-Quiles and J. Nelson, *Adv. Funct. Mater.*, 2014, DOI: 10.1002/adfm.201401626.

40 40. J. A. Lim, F. Liu, S. Ferdous, M. Muthukumar and A. L. Briseno, *Materials Today*, 2010, **13**, 14-24.

41 41. E. K. Fleischmann and R. Zentel, *Angewandte Chemie - International Edition*, 2013, **52**, 8810-8827.

42 42. C. Poelking and D. Andrienko, *Macromolecules*, 2013, DOI: 10.1021/ma4015966.

43 43. X. Lu, H. Hlaing, D. S. Germack, J. Peet, W. H. Jo, D. Andrienko, K. Kremer and B. M. Ocko, *Nat Commun*, 2012, **3**, 795.

44 44. N. Blouin, A. Michaud, D. Gendron, S. Wakim, E. Blair, R. Neagu-Plesu, M. Belletête, G. Durocher, Y. Tao and M. Leclerc, *Journal of the American Chemical Society*, 2007, **130**, 732-742.

45 45. O. Bubnova and X. Crispin, *Energy and Environmental Science*, 2012, **5**, 9345-9362.

46 46. G. J. Snyder and E. S. Toberer, *Nat Mater*, 2008, **7**, 105-114.

47 47. O. E. Parfenov and F. A. Shklyaruk, *Semiconductors*, 2007, **41**, 1021-1026.
48 48. A. Weathers, Z. U. Khan, R. Brooke, D. Evans, M. T. Pettes, J. W. Andreasen, X. Crispin and L. Shi, *Adv Mater*, 2015, **27**, 2101-2106.
49